Small hydrocarbon particle erosion in a hot gas

M. Bocchio, E. Micelotta, A.-L. Gautier, A. Jones

A&A 545, A124 (2012)
DOI: 10.1051/0004-6361/201219705

Astronomy & Astrophysics

Small hydrocarbon particle erosion in a hot gas

A comparative study

M. Bocchio[1], E. R. Micelotta[2], A.-L. Gautier[3], and A. P. Jones[1]

[1] Institut d'Astrophysique Spatiale (IAS), UMR 8617, CNRS/Université Paris-Sud, 91405 Orsay, France
e-mail: marco.bocchio@ias.u-psud.fr
[2] Department of Physics and Astronomy, Western University, London, Ontario N6A 3K7, Canada
[3] LESIA, Observatoire de Paris, CNRS, UPMC, Université Paris Diderot, Paris Sciences et Lettres, 5 place Jules Janssen, 92195 Meudon, France

Received 29 May 2012 / Accepted 12 July 2012

ABSTRACT

Aims. We compare the classical and molecular approaches for small particle erosion, in an overlapping particle size domain, to model dust destruction in a hot gas.
Methods. We calculated and compared the carbon ejection rate constant for a-C:H grains and PAHs (with 50 to 5000 carbon atoms) in a hot gas (10^4–10^8 K).
Results. The classical approach does not take into account electron collisions nor electronic interactions, which are shown, using the molecular approach, to be important for small grains ($\lesssim$1000 carbon atoms). For $N_C \leq 1000$ the two approaches diverge but for larger grains they are in very good agreement for a wide range of temperatures ($T \approx 10^5$–10^7 K).
Conclusions. To quantify the erosion of small hydrocarbon grains in a hot gas a molecular approach, rather than classical sputtering, needs to be adopted. This then indicates that small hydrocarbon nano-particles (with $N_C < 1000$ or $a < 3$ nm) cannot be abundant in a hot coronal-type gas, be it galactic hot ionised medium or nearby intergalactic medium, because they are rapidly destroyed by dissociation resulting from electronic excitations induced by electron collisions.

Key words. ISM: general – dust, extinction – Galaxy: halo – galaxies: clusters: intracluster medium

1. Introduction

In a hot gas, dust particles undergo erosion because of the collision with the energetic ions in the gas. This process is known as thermal sputtering. The thermal sputtering of dust in the interstellar medium (ISM) is only important for gas kinetic temperatures, T_k, greater than 10^6 K (e.g., Draine & Salpeter 1979; Jones 2004) and is therefore unimportant in "cold" ISMs media such as photodissociation regions, HII regions and in the warm intercloud medium with $T_k \simeq 10^4$ K. Thus, it is only in a low-density ($n_H \simeq 10^0$–10^{-4} cm^{-3}) hot coronal-type gas ($T_k \simeq 10^6$–10^8 K), such as in the hot ionised medium (HIM) of galaxies or in the intergalactic medium (IGM, $n_H \simeq 10^{-2}$–10^{-4} cm^{-3}), that thermal sputtering is an important process.

In this paper we re-visit the problem of small hydrocarbon particle erosion and, in particular, consider the effects of electron collisions and electronic interactions.

2. Thermal sputtering

2.1. Carbon grain erosion

The thermal erosion of grains in a hot gas is well described by the approach followed by Tielens et al. (1994). They found an analytical result for the thermal erosion, which they compared to the experimental studies of sputtering of a variety of materials, and considered the gas as mainly composed by H^+, He^+, and the CNO group ions in the temperatures range $T \approx 10^4$–10^8 K. In this work, the target was considered to be a semi-infinite planar surface, even if, as we will see in the following section, the finiteness of the grains must be taken into account for a more precise analysis. The impacts of the incident ions create a collisional cascade inside the target (taken into account in the model of the sputtering yield, i.e. the number of sputtered atoms per incident particle) and, depending on the temperature of the gas, they can have enough energy and momentum to break the bonds of the surface atoms. In this way the target grain is eroded by the ambient gas.

Table 1. Parameters for target and projectile materials.

Projectile parameters				
Material	M_1	χ		
H	1.0	1.0		
He	4.0	0.1		
C	12.0	10^{-4}		
Target parameters				
Material	U_0	K	ρ	X_H
a-C	4	0.65	2.2	0
a-C:H	4	–0.04	1.4	0.4

Notes. M_1 is the mean atomic mass of the projectile (amu), χ the abundance, U_0 the surface cohesion energy (eV), K a free parameter, ρ the density (g cm^{-3}) and X_H the atomic fraction of hydrogen in the particle.

We calculate the sputtering yield using the parameters in Table 1 for projectile and target materials for hydrogenated amorphous carbon (a-C:H) and amorphous carbon (a-C) as per the approach of Tielens et al. (1994) but as updated by Serra Díaz-Cano & Jones (2008). We adopt a carbon abundance $\chi_C = 10^{-4}$, which is an intermediate value between what has been estimated by Sofia & Parvathi (2009) and Cardelli et al. (1996). The

inclusion of nitrogen and oxygen into the sputtering calculation does not change our results. From the sputtering yield we can calculate the carbon ejection rate,

$$\frac{\mathrm{d}N_{\rm sp}}{\mathrm{d}t} = 2\pi a^2 \sum_i n_i \langle Y_i v \rangle \quad (1)$$

where $N_{\rm sp}$ is the number of sputtered atoms, the factor 2 takes into account the average of the yield over all angles of incidence, $n_i = n_{\rm H}\chi_i$ is the density of a given projectile with abundance χ_i, $n_{\rm H}$ is the proton density and

$$\langle Y_i v \rangle = \int Y_i v f(v) \mathrm{d}v \quad (2)$$

with Y_i the sputtering yield for a given projectile, v the projectile velocity and $f(v)$ the Maxwell-Boltzmann velocity distribution at the given gas temperature. The target carbon atom ejection rate constant is given by $\mathrm{d}N_{\rm sp}/\mathrm{d}t/n_{\rm H}$.

The parameters (see Table 1) used for a-C:H grains differ a little from the ones for the amorphous carbon (a-C) and the finiteness of the grains has been taken into account as per Serra Díaz-Cano & Jones (2008), see Appendix A.

The number of carbon atoms in an a-C:H grain is given by:

$$N_{\rm C} = \frac{4\pi\rho N_{\rm A} a^3}{3 \times [(1 - X_{\rm H})M_{\rm C} + X_{\rm H} M_{\rm H}]} (1 - X_{\rm H}) \quad (3)$$

where a is the grain radius, $N_{\rm A}$ the Avogadro's number, ρ the grain density, $X_{\rm H}$ the atomic fraction of hydrogen in the particle, i.e. $X_{\rm H} = N_{\rm H}/(N_{\rm C} + N_{\rm H})$ (ρ and $X_{\rm H}$ are given in Table 1), and $M_{\rm C}$ and $M_{\rm H}$ the atomic masses of carbon and hydrogen atoms respectively ($M_{\rm C} = 12$ and $M_{\rm H} = 1$).

2.2. PAH erosion

To describe the erosion of polycyclic aromatic hydrocarbons (PAHs) by ions and electrons in a hot gas, we adopt the molecular model developed by Micelotta et al. (2010a,b).

The interaction of a PAH molecule with an ion consists of two simultaneous processes which can be treated separately: the transfer of energy to a single carbon atom of the PAH through a binary collision with the projectile ion (*nuclear stopping* or *elastic energy loss*) and the energy loss due to the PAH electron cloud (*electronic stopping* or *inelastic energy loss*). If the energy transferred through nuclear stopping exceeds the nuclear threshold energy T_0, the target carbon will be ejected from the molecule. The standard value adopted for T_0 is 7.5 eV. The energy transfer through electronic stopping is described in terms of the stopping power S of an electron gas with appropriate density. The stopping power is defined as the energy loss per unit length: $S = \mathrm{d}T/\mathrm{d}s$, where $\mathrm{d}T$ is the energy loss over the pathlength $\mathrm{d}s$.

For PAH collisions with electrons the energy transfer occurs through inelastic interactions with the target electrons, as for electronic excitation. The electron stopping power has been derived from measurements of $\mathrm{d}T/\mathrm{d}s$ in solid carbon Micelotta et al. (2010a,b).

The energy transferred through electronic interactions and electron collisions is spread over the entire molecule. The result is a collective excitation of the PAH, followed eventually by fragmentation or radiative relaxation. The dissociation probability is governed by the parameter E_0, which describes the dissociation rate of a highly excited PAH molecule using an Arrhenius law. The value adopted for E_0 is 4.6 eV (Micelotta et al. 2010a,b).

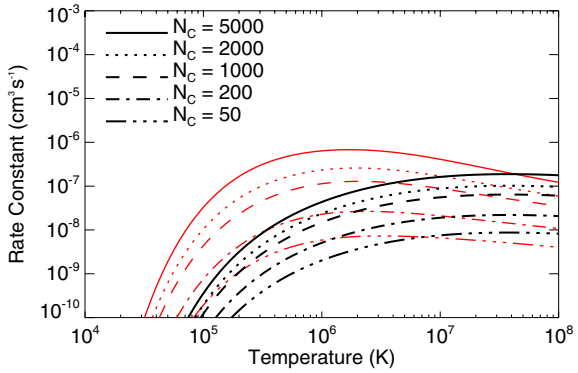

Fig. 1. $\mathrm{d}N_{\rm sp}/\mathrm{d}t/n_{\rm H}$. Comparison between a-C (black) and a-C:H (red) sputtering due to H^+, He^+ and C^+ projectiles.

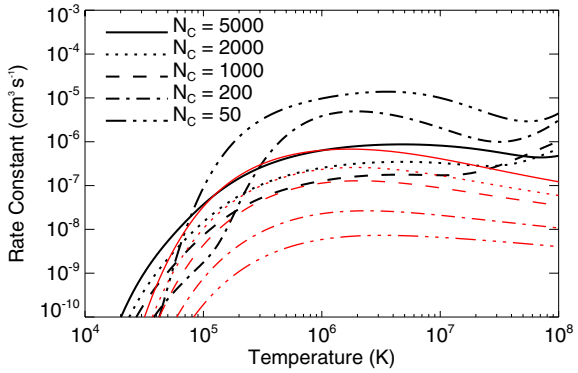

Fig. 2. $\mathrm{d}N_{\rm sp}/\mathrm{d}t/n_{\rm H}$. Comparison between PAH (black) and a-C:H (red) sputtering due to H^+, He^+, C^+ and electrons (only for PAHs) projectiles.

The destructive effects on PAHs of collisions with ions and electrons in a thermal gas are described in terms of the rate constant for carbon atom ejection, which is defined by the ratio between the carbon ejection rate and the density of hydrogen nuclei $n_{\rm H}$. The carbon ejection rate is derived using Eqs. (8) and (23) in Micelotta et al. (2010b). The results of the PAH erosion model are exemplified in Fig. 8 in Micelotta et al. (2010b). The curves clearly show that electrons are the most important destruction agents for small PAHs (50 carbon atoms), while the erosion of large PAHs (1000 carbon atoms) is dominated by nuclear interaction.

3. Results

In Fig. 1 we compare the sputtering rate constants of Tielens et al. (1994) and Serra Díaz-Cano & Jones (2008) for different gas temperatures and for different grain sizes expressed as $N_{\rm C}$. We notice that the use of different parameters for a-C:H and the size effect (more important for high temperatures) taken into account to calculate the sputtering yield do change the profile of the sputtering rate quite significantly.

In Fig. 2 we compare the thermal sputtering for PAHs and a-C:H grains. For the PAHs we use the molecular approach (Micelotta et al. 2010b), while for a-C:H grains we use the classical approach (Serra Díaz-Cano & Jones 2008) with the size effect included. We see that for the a-C:H model the sputtering rate constant increases with the increasing number of carbon atoms ($N_{\rm C}$), while for the PAH model the behavior changes at $N_{\rm C} \approx 1000$. For $N_{\rm C} \gtrsim 1000$ the sputtering rate constant increases as $N_{\rm C}$ increases, as per a-C:H, but for $N_{\rm C} \lesssim 1000$ it increases

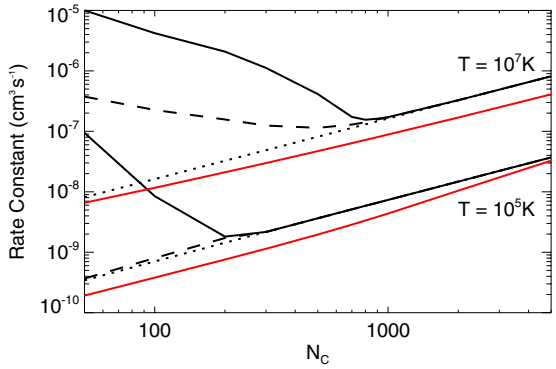

Fig. 3. $dN/dt/n_H$ at $T = 10^5$ K and at $T = 10^7$ K. Red line: rate constant for a-C:H grains. Black lines: rate constant for PAHs; the dotted line shows nuclear interaction only, the dashed line the summed effects of nuclear and electronic interactions, whilst the solid line includes electron collisions as well. The results for $T = 10^6$ K are not shown here but are very similar to those for $T = 10^7$ K.

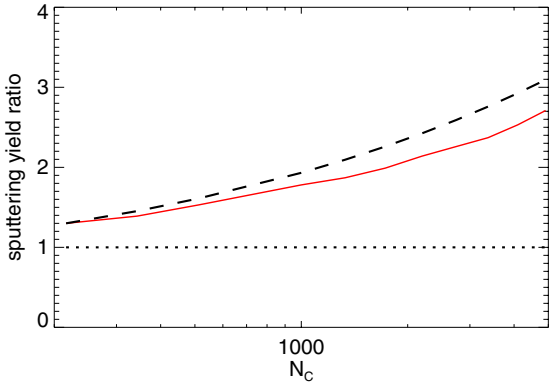

Fig. 4. Red solid line: ratio between the number of sputtered atoms in the 3D case (obtained by our simple model of collisional cascade for $T = 10^7$ K) and the single atoms ejected in the PAH case (considering only the nuclear interaction above threshold). Black dashed line: ratio between the geometrical cross-section of a planar PAH and that of a 3D a-C:H grain. The x axis shows the number of carbon atoms in the particle.

as N_C decreases. For $N_C \gtrsim 1000$ the two models agree for temperatures $T = 10^5$–10^6 K and within a factor of about 2 for $T = 10^7$ K. On the other hand they lead to different results for small grains, which is clearer in the following plot (Fig. 3) where we show the carbon ejection rate constant for a-C:H grains (red lines) and PAHs (black line) for gas temperatures $T = 10^5$ K and $T = 10^7$ K as a function of the number of carbon atoms in the grain/molecule.

The dotted black line (in Fig. 3) shows the sputtering due to nuclear interaction (binary collision) only, the dashed one represents the sputtering due to both nuclear and electronic interactions, whilst the black solid line includes electron collisions as well. The effect of collisions between electrons and the particles is remarkable for grains with a small number of carbon atoms. In the absence of electron collisions and electronic interactions the two models would be very close, regardless of the gas temperature in this range. We can see that, for $N_C \gtrsim 1000$ (for $T = 10^7$ K), the electron collisions and the electronic interactions are negligible in the approach used to treat the PAHs. In the classical model described by Tielens et al. and Serra Díaz-Cano and Jones electron collisions are not taken into account but they clearly will be important for particles with a sufficiently small number of carbon atoms.

The other important fact here is the extremely good accordance between the classical model and the nuclear interaction of the PAH model. This can be seen as the combination of two different effects. In the classical approach, since we consider 3D grains, a collisional cascade contributes to the sputtering yield allowing the possibility of ejecting more than one target atom. On the other hand, in the PAH approach there is no such effect, because only binary collisions are considered, but the cross-section increases with the number of carbon atoms more rapidly than in the 3D case.

In the molecular approach, if we consider only the nuclear interaction, which is represented by the dotted lines in Fig. 3, we only have binary collisions. If the transferred energy in the collision is higher than a certain threshold energy, $T_0 = 7.5$ eV, then this leads to a loss of a single carbon atom. We would expect that, in the classical approach, the enhancement of the sputtering yield due to the collisional cascade compensates for the enhancement of the sputtering yield in the molecular approach due to the difference in cross-section. In order to investigate this we built a simple model of collisional cascade. Grains are modeled as cubes where the carbon atoms occupy fixed positions and are treated as hard spheres. We considered only binary collisions between atoms and we used an energy-dependent nuclear cross-section as described in (Micelotta et al. 2010a, Eq. (15))[1]. As an initial projectile we took a proton with an energy distribution given by the Maxwell-Boltzmann energy distribution at the temperature $T = 10^7$ K. We allowed multiple collisions and for each collision we consider a threshold energy $T_0 = 7.5$ eV. For each angle and input energy we counted the sputtered atoms only if the first proton transferred an energy larger than the threshold energy. Then we averaged over all the possible angles and over the Maxwell-Boltzmann energy distribution. In Fig. 4 we show (red solid line) the ratio between the number of sputtered atoms due to collisional cascade in a 3D a-C:H grain and that for a PAH molecule (i.e. single sputtered atoms for the molecular case for a transferred energy larger than 7.5 eV) as a function of the number of carbon atoms in the particle. We see that, the larger the grain is the more important the cascade will be and consequently the larger the number of sputtered atoms. On the other hand, the geometrical cross-section of a 2D PAH for a given number of carbon atoms is larger than that of a 3D grain. This difference in the geometrical cross-section leads to an enhancement in the sputtering yield in the molecular approach with respect to the classical one.

The expression for the radius of an a-C:H grain can be derived from Eq. (3), whilst the relation between the radius of a PAH molecule and the number of carbon atoms is given by the following equation:

$$a(\mathrm{nm}) = 0.09\ \sqrt{N_C} \tag{5}$$

where a is the radius of the PAH in nm. If we consider a PAH as a thick disk of radius a and thickness $d = 0.3354$ nm then its geometrical cross-section, averaging over all angles, will be

$$\sigma_{\mathrm{PAH}} = \frac{\pi}{2}\left(a^2 + ad\right) \tag{6}$$

[1] It should be noted that Eq. (13) in the article should be:

$$m(E) = 1 - \exp\left[-\exp\left[\sum_{i=0}^{5} a_i \left(0.1 \ln\left(\frac{\epsilon(E)}{\epsilon_1}\right)\right)^i\right]\right] \tag{4}$$

as indicated in Ziegler et al. (1985).

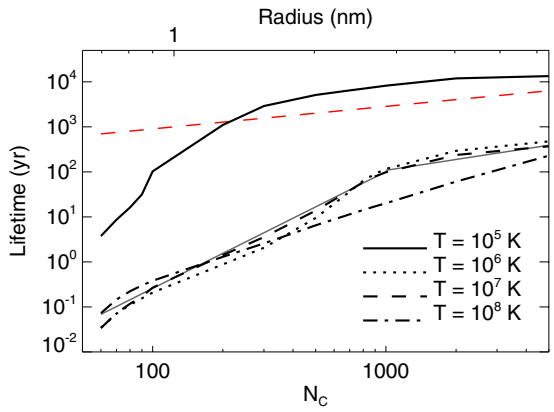

Fig. 5. PAH lifetime (in years) as a function of the number of carbon atoms, N_C, in the particle for a gas phase proton density $n_H = 1\,cm^{-3}$ and for temperatures of 10^5 (solid line), 10^6 (dotted line), 10^7 (dashed line) and 10^8 K (dash-dot line). The fit (see text for details) for the case $T = 10^7$ K is shown in gray solid line. We can compare our fit to previous estimates (Draine & Salpeter 1979; Jones 2004), which are shown in red dashed line (see text for details).

So the ratio between the two cross-sections is given by:

$$\frac{\sigma_{PAH}}{\sigma_{aCH}} = \frac{1/2\,\pi(a_{PAH}^2 + a_{PAH}d_{PAH})}{\pi a_{aCH}^2}$$

$$= \frac{9\times10^{-9}(9\times10^{-9}N_C^{1/2} + 3.4\times10^{-8})\,[4\pi\rho N_A(1-X_H)]^{2/3}}{2\times3^{2/3}N_C^{1/6}[(1-X_H)M_C + X_H M_H]^{2/3}} \quad (7)$$

where a_{PAH} and a_{aCH} are the radii for a PAH and aCH grain, ρ is expressed in g cm^{-3}, M_C and M_H in amu. In Fig. 4, the black dashed line gives the ratio between the PAH cross-section and the 3D grain cross-section as a function of the number of carbon atoms in the particle. We can see that, even with a simple model like this, the behaviours of the red solid line and the dashed black one are similar. This means that the effect of the cross-section compensates the effect of the collisional cascade in 3D grains. This would explain the agreement between the sputtering rate constants for the two models.

Thus, the molecular approach of Micelotta et al. (2010a,b) can and should be used when considering the erosion of any small hydrocarbon particles, be they PAHs or a-C:H grains, in a hot gas because the classical sputtering approach, extended to particles with less than ~1000 carbon atoms, does not take into account electronic excitation effects and thus underestimates the degree of destruction.

4. Astrophysical implications

Considering a hydrocarbon particle (PAH or 3D a-C:H grain) of a given size we can follow its time-dependent evolution using the equation below:

$$t - t_0 = \int_{N_C(t_0)}^{N_C(t)} \frac{dN_C}{dN_C/dt} \quad (8)$$

where dN_C/dt is the ejection rate calculated in the previous sections. The time t_{dest} when the grain/molecule is totally dissociated corresponds to its life-time. At $t = t_{dest}$, we have $N_C(t_{dest}) = 0$. In Fig. 5 we show the PAH life-time as a function of the number of carbon atoms, N_C, in the molecule for unit proton density and gas temperatures of 10^5, 10^6, 10^7 K and 10^8 K. It should be noted that hydrocarbon particles with $N_C \leqslant 5000$ have radii $\lesssim$7 nm.

In the hot post-shock gas behind a fast shock ($T_k \sim 5\times10^5$ K and $n_H \sim 1\,cm^{-3}$) the hydrocarbon nano-particle life-time will be $<10^3$ yr, which is consistent with the results of Jones et al. (1996) for 200 km s^{-1} shocks. Nevertheless, our results indicate that, in such shocks, the thermal sputtering of hydrocarbon nano-particles should be even more pronounced than in this earlier work. However, and given that in the Jones et al. (1996) study, thermal sputtering was already the dominant destruction process for small carbon grains, our new erosion rates do not qualitatively change their results.

In the HIM or IGM, with $n_H \simeq 10^{-2}$–$10^{-4}\,cm^{-3}$ and $T_k = 10^6$–10^7 K, Fig. 5 indicates hydrocarbon nano-particle lifetimes of $<10^7$, $<10^6$ and $<10^5$ yr, for $n_H \simeq 10^{-4}$, 10^{-3} and $10^{-2}\,cm^{-3}$, respectively. For typical IGM conditions, i.e., $n_H \simeq 10^{-3}\,cm^{-3}$ and $T_k = 10^7$ K, the hydrocarbon nano-particle life-time, t_{dest}, is less than a thousand years and the exact size-dependent life-times can be approximated by (gray solid lines in Fig. 5):

$$t_{dest} \approx 2\times10^{-6}\,\frac{N_C^{2.6}}{n_H/cm^{-3}}\ \text{yr} \quad \text{for } N_C \leqslant 1000$$

$$\approx 0.43\,\frac{N_C^{0.8}}{n_H/cm^{-3}}\ \text{yr} \quad \text{for } N_C > 1000\ (\equiv a \gtrsim 3\,\text{nm}). \quad (9)$$

For PAHs with $N_C \geqslant 1000$ the above expression is equivalent to

$$t_{dest} \approx \frac{20\,a(\text{nm})^{1.6}}{n_H/cm^{-3}}\ \text{yr} \quad \text{for } a \gtrsim 3\,\text{nm}, \quad (10)$$

where a is the PAH radius in nm. These life-times show a stronger size-dependency than previous estimates, i.e., $t_{dest} \approx 10^3\,a(\text{nm})/(n_H/cm^{-3})$ yr (Draine & Salpeter 1979; Jones 2004), see red dashed line in Fig. 5.

In the calculation of the particle life-times, the sputtering rate plays a central role. As is clearly shown in Fig. 3, the addition of electron collisional sputtering and electron interaction in our calculations dramatically increases the sputtering rate for small particles. As a consequence, we have that the particle life-times are shorter than the previous estimates, which were based on the presumed dominance of proton sputtering in the hot gas and only the nuclear interaction was taken into account. Evidently, for small particles (i.e., $N_C < 1000 \equiv a \lesssim 3$ nm), the destruction time-scale is significantly shorter than the previous estimates and, additionally, shows a stronger size-dependence.

From Eq. (8), we can also calculate the time-dependent evolution for a grain of a given size. In Fig. 6, we show the time-dependent evolution of a hydrocarbon grain initially of 5000 carbon atoms in a gas with unit proton density and temperature of 10^5 (solid line), 10^6 (dotted line), 10^7 (dashed line) and 10^8 K (dash-dot line). The time-dependent evolution of grains with $N_C < 5000$ can be seen as a shift in time of the plot in Fig. 6. For example a 5000 carbon atoms PAH in a gas at $T = 10^7$ K evolve with time as indicated in Fig. 6 (dashed line) and at a time $t_0 \approx 2.5\times10^2$ yr it contains only 1000 carbon atoms. The time-dependent evolution of a 1000 carbon atoms PAH is given by the same line in Fig. 6 but starting from t_0.

5. Conclusions

We find that the PAH, or molecular, approach to hydrocarbon nano-particle erosion provides an excellent means of determining the processing of 3D particles with the same number of carbon atoms. This approach indicates that electronic interactions

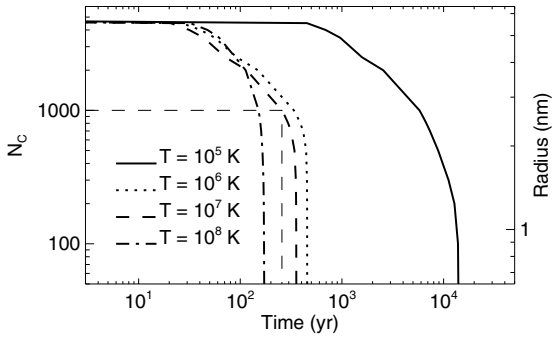

Fig. 6. The time-dependent evolution of PAHs, with $N_C = 5000$, for a gas phase proton density $n_H = 1\,cm^{-3}$ and for temperatures of 10^5 (solid line), 10^6 (dotted line), 10^7 (dashed line) and 10^8 K (dash-dot line).

and electron collisions are important for particles with fewer than about 1000 carbon atoms and must be taken into account in determining hydrocarbon nano-particle life-times in a hot gas.

From our study it appears that hydrocarbon nano-particles (with $N_C < 1000$ or $a < 3\,nm$) cannot be abundant in a hot coronal-type gas, be it galactic HIM or nearby IGM (e.g. $t_{dest} \leqslant 10^6$ yr for $T = 10^6$–10^7 K and $n_H = 10^{-3}\,cm^{-3}$). Thus, it is to expected that any dust emission coming from the HIM of a galaxy or from the IGM in the close proximity of a galaxy must be dominated by emission from large hydrocarbon grains with life-times $>10^8$ yr (see Eq. (10)), with radii $>100\,nm$, or perhaps more likely from amorphous silicate grains that appear to be more resistant to thermal sputtering than carbonaceous dust (e.g., Jones et al. 1996). We have not re-evaluated the effects of amorphous silicate thermal sputtering here but, in the light of important small particle sputtering effects apparent in hydrocarbon dust (Serra Díaz-Cano & Jones 2008), the size-dependent sputtering effect will need to be carefully evaluated for amorphous silicate dust as well.

Acknowledgements. E.R.M. wishes to acknowledge the support from the National Science and Engineering Research Council of Canada (NSERC). We would like to thank the anonymous referee for his useful comments and suggestions.

Appendix A: a-C:H size-dependent sputtering yield

In the model described by Serra Díaz-Cano & Jones (2008) they used a size-dependent sputtering yield given by:

$$Y/Y_\infty = 1 + 6.6\exp\left[\frac{-\log^2\left(\frac{a/R_d}{a_0}\right)}{2\sigma^2}\right] - \exp\left(-(7a/R_d + 0.25)^2\right) \quad (A.1)$$

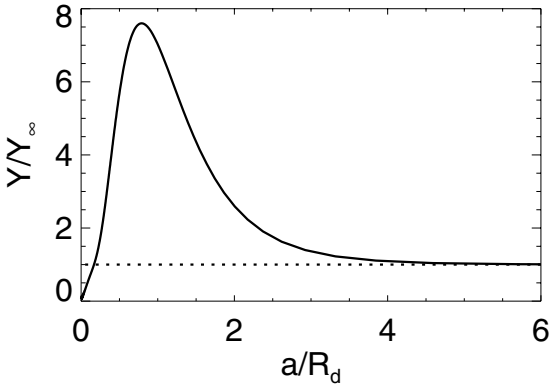

Fig. A.1. Correction to the sputtering yield taking into account the finiteness of grains.

where Y_∞ is the sputtering yield in the case where the grain is considered as a semi-infinite plane, a is the radius of the grain, $R_d = R_p/2$, where R_p is the implanting depth (see Eq. (A.2)), $\sigma = 0.552$ and $a_0 = 0.79$.

$$R_p = \left(\frac{-8.0}{E} + 0.1357\,E + 7.601\right)\,(nm) \quad (A.2)$$

with E the energy of the impinging ion in eV.

As we can see in Fig. A.1, the sputtering yield ratio Y/Y_∞ is smaller than 1 for small grain radii, which means that the ions actually pass through the grain for sufficiently large energies, when the implanting depth is larger than the radius of the grain. At $a \approx R_p$ there is an enhancement in the sputtering yield ratio whilst it tends to 1 for large values of a/R_d (>4), which means that the semi-infinite plane model approximation starts to be valid.

References

Cardelli, J. A., Meyer, D. M., Jura, M., & Savage, B. D. 1996, ApJ, 467, 334
Draine, B. T., & Salpeter, E. E. 1979, ApJ, 231, 77
Jones, A. P. 2004, in Astrophysics of Dust, eds. A. N. Witt, G. C. Clayton, & B. T. Draine, ASP Conf. Ser., 309, 347
Jones, A. P., Tielens, A. G. G. M., & Hollenbach, D. J. 1996, ApJ, 469, 740
Micelotta, E. R., Jones, A. P., & Tielens, A. G. G. M. 2010a, A&A, 510, A36
Micelotta, E. R., Jones, A. P., & Tielens, A. G. G. M. 2010b, A&A, 510, A37
Serra Díaz-Cano, L., & Jones, A. P. 2008, A&A, 492, 127
Sofia, U. J., & Parvathi, V. S. 2009, in Cosmic Dust – Near and Far, eds. T. Henning, E. Grün, & J. Steinacker, ASP Conf. Ser., 414, 236
Tielens, A. G. G. M., McKee, C. F., Seab, C. G., & Hollenbach, D. J. 1994, ApJ, 431, 321
Ziegler, J. F., Biersack, J. P., & Littmark, U. 1985, The Stopping and Ranges of Ions in Matter, ed. J. F. Ziegler (Pergamon Press), 1